International Journal of Fatigue 162 (2022) 106990

Contents lists available at ScienceDirect

International Journal of Fatigue

journal homepage: www.elsevier.com/locate/ijfatigue

Influence of deformation prior to ageing on fatigue behavior of extruded AA6082-T6 profiles

Xintong Wang [a], Jun Ma [b,*], Torgeir Welo [b,**]

[a] Centre for Autonomous Marine Operations and Systems, Department of Marine Technology, Norwegian University of Science and Technology, Trondheim 7491, Norway
[b] Department of Mechanical and Industrial Engineering, Norwegian University of Science and Technology, Trondheim 7491, Norway

ARTICLE INFO

Keywords:
Extruded aluminum profile
High-cycle fatigue
Pre-deformation
Artificial ageing

ABSTRACT

This paper investigates the effect of plastic deformation before artificial ageing on fatigue behavior of extruded AA6082-T6 profiles. As-received, T4-temper materials are pre-deformed at different strains and followed by artificial ageing to T6-temper, simulating industrial manufacturing route of aluminum components. Load controlled, high-cycle fatigue tests are conducted for deformed, aged specimens to explore their fatigue behavior. An 18–23% increase in fatigue life is achieved by pre-straining of 5–15% in T4-temper, as compared to that without pre-straining. Furthermore, the designed manufacturing route provides a transient cyclic softening stage for AA6082 samples. The pre-strained material provides a larger cycle softening during fatigue.

1. Introduction

With today's increased focus on environmental impact, more lightweight and sustainable products are highly demanded in the marine industry. Using aluminum alloys with high strength-to-weight ratios is one of the most important contributors for increasing energy efficiency of marine structures in operational phases. In addition, excellent recyclability of aluminum alloys also contributes to less CO_2 emissions during the life cycle compared to other alternatives. Therefore, aluminum alloys can provide increased applicability in marine structures such as high-speed vessels, helicopter decks, gangways, etc. One particular technology example is aluminum extrusions combined with friction stir welding to enable the fabrication of integrally-stiffened structures, which contribute to fewer welding operations, lower cost, and higher product performance in different application areas.

During the manufacturing process, various thermo-mechanical parameters and their interactions make it hard to predict and control the mechanical properties of the final products. Significant efforts have been made to understand the thermo-mechanical effects on microstructures and static mechanical properties of aluminum alloys [1–6], and many other alloys such as titanium [7–9], and so on. Previous research has also investigated the influence of processing history on fatigue behavior of aluminum alloys, e.g., with focus on cast, hot isostatic pressing (HIP) and equal-channel angular pressing (ECAP) processes [10–17]. It was found that the processing history largely influences the microstructure and thus the fatigue behavior of aluminum alloys. The fatigue behavior was identified as particularly sensitive to plastic deformation (pre-deformation) during forming and the subsequent heat-treatment (post-thermal-treatment).

In most of the research up to now, the effects of pre-deformation and heat treatment on the fatigue behavior of aluminum alloy components have been investigated separately. Different, occasionally inconclusive, conclusions have been drawn concerning the effect of deformation, depending on the material compositions, pre-straining levels, material orientations, etc. Several studies suggest that the pre-strain will decrease the fatigue life [18–25], while other studies indicate that the fatigue life will remain at the same level as that of the undeformed material [21,22], and in some cases even increase [16,17,25]. Concerning thermal treatment effects, most research reveals that the fatigue performance could be improved due to the precipitation hardening of aluminum alloys. The particular improvement depends on the heat-treatment method and specific process parameters [26–34].

In the case of combined effects of pre-deformation and post-thermal-treatment, several experimental studies have been conducted for various aluminum alloys, but with somewhat different outcomes. For example, the fatigue life decreased for ultrafine-grained AA6060 aluminum alloys [35], but remained at the same level for 7000-series aluminum alloys [36]. Liu et al. [37] studied the fatigue behavior of samples of rolled Al-

* Corresponding author.at: Richard Birkeland's vei 2B, Trondheim 7491, Norway.
** Corresponding author.at: Richard Birkeland's vei 2B, Trondheim 7491, Norway.
E-mail addresses: jun.ma@ntnu.no (J. Ma), torgeir.welo@ntnu.no (T. Welo).

https://doi.org/10.1016/j.ijfatigue.2022.106990
Received 18 November 2021; Received in revised form 12 April 2022; Accepted 5 May 2022
Available online 10 May 2022
0142-1123/© 2022 The Authors. Published by Elsevier Ltd. This is an open access article under the CC BY-NC-ND license (http://creativecommons.org/licenses/by-nc-nd/4.0/).

Cu-Li alloys with pre-deformation and ageing. The study shows that the pre-deformed material provides a greater damage resistance compared to the non-deformed material. Zhang et al. [38] studied the effects of pre-deformation and artificial ageing on the fatigue life of AA2198 Al-Li alloy. It is found that the micro-crack defects from the pre-deformation could lead to a decrease in fatigue life, where the decrease is proportional to the pre-strain level. Samples with 3% pre-deformation were aged at 155 °C for 15 h and showed improved fatigue life and damage resistance compared to ones with 1% and 5% pre-deformation. For AA6082 aluminum alloy used in marine applications, the investigation of the combined effect of deformation and thermal treatment is crucial as this is the basis for any manufacturing route for this type of components. Generally, aluminum alloy profile-based components are extruded, formed, and heat-treated to achieve the desired dimensional configuration and properties [39,40]. Fatigue design and assessment are normally based on the properties of undeformed material. However, plastic deformation after forming is nonuniformly distributed with different levels in different regions of the formed parts. The magnitude of plastic strain can also be at a very high level locally. Thus, it is intuitive that the deformation history may influence the fatigue behavior of the final product, even after artificial ageing. Once understood in detail, these effects should therefore be taken into account in the design of products and manufacturing routes.

To bridge the research gap identified above, a thermo-mechanical processing route is designed to simulate conditions in industrial manufacturing processes. The aim is to improve the understanding of how the fatigue behavior of AA6082-T6 alloys is affected by pre-strain generated in T4-temper, if any, hence supporting the design of safer and more sustainable aluminum products, as well as more optimal processing routes. To this end, different pre-strain levels are introduced to AA6082 specimens in T4-temper by uniaxial tension, before artificially ageing these pre-deformed samples to T6 temper. Then, both static tensile and high-cycle fatigue tests are conducted on the different samples. The fracture surface of the fatigue specimens is analyzed using a scan electron microscope (SEM) technique. The static mechanical properties, fatigue life cycles and cyclic hardening/softening behavior due to the combined effects of pre-deformation and artificial ageing are analyzed in detail.

The remainder of this paper is structured as follows: First, the experimental procedures are described in Section 2. Section 3 introduces the results from the static tensile testing and fatigue testing of the samples exposed to different thermo-mechanical histories, followed by a discussion of the findings supported by the results from SEM observations. Finally, the main conclusions are presented in Section 4.

2. Materials and methods

The material used in this study is AA6082-T4 aluminum alloy provided by Hydro ASA. The nominal chemical composition of the material is shown in Table 1. The engineering stress-strain curve of the received material is obtained by uniaxial tensile tests, as shown in Fig. 1.

The experimental methodology and geometrical dimensions of the specimens are illustrated in Fig. 2. The AA6082-T4 material is supplied as rectangular hollow sections, which are hot extruded, quenched, and natured aged to T4 temper. The width of the original section is 60 mm, the depth is 40 mm, and the nominal thickness is 3 mm. The flat tensile specimens are prepared from the middle area of the extrusions by a water jet cutter and subsequent machining.

The pre-strain is introduced to the flat tensile specimens in T4-temper using a uniaxial tensile test set-up. Four nominal strain levels,

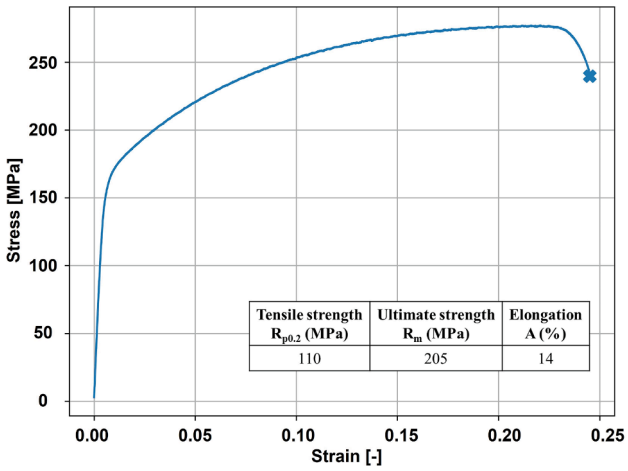

Fig. 1. Engineering stress-strain curve of the as-received AA6082-T4 extruded profile. The fracture point is marked with the cross. Main mechanical properties are also listed.

i.e., 0% (no pre-strain before ageing), 5%, 10%, and 15% are set by displacement-controlled tensile tests. The introduced pre-strains are selected based on the uniform deformation stage of the stress–strain curve, thereby avoiding any potential effect of local deformations (necking). An MTS Landmark hydraulic test machine (50 kN) is used for the tests at a speed of 3 mm per minute (nominal strain rate of about 10^{-3} per second) at room temperature. An Instron-2620 extensometer with a 50 mm gauge length is used to measure the strain during tension.

After polishing, the tensile specimens are artificially aged at 180 °C for eight hours for providing a T6-temper, corresponding to standard industrial practice [42]. The fatigue specimens are then prepared by machining according to ASTM E466 [43]. High-cycle fatigue tests are applied by the same MTS machine used for pretension, employing the load-controlled mode. A sinusoidal stress history is applied in the fatigue test. The stress range of 250 MPa is determined by the uniaxial tensile tests and fatigue test runs, adjusting the fatigue life to the high-cycle range (i.e., above 10^4 cycles), while balancing the experimental time and cost. A stress ratio of R = 0.1 is used to ensure suitable fracture surfaces for subsequent SEM observations. The stress frequency is set as f = 30 Hz. The thickness change of the sample after tension was measured by a caliper gauge to obtain the corresponding elastic stress levels according to the correct cross-section area of each fatigue specimen. For each experimental test combination, five repeated tests are carried out to provide more reliable results of cycle numbers. Complete separation of the specimen is regarded as the failure criterion. The data are collected through a PC-based acquisition system with a frequency of 600 Hz, representing 20 recordings for each cycle.

To investigate the fractography of the fatigue specimens for more in-depth analyses at microstructural level, SEM tests are performed using a Quanta 650 FEG SEM (Thermo Fisher Scientific Inc.). The accelerating voltage was 20 kV, with a working distance of around 35 mm, an aperture of 30 μm and a spot size of 3.0.

3. Results and discussions

3.1. Static mechanical properties

The engineering stress-strain curves of AA6082 after pre-

Table 1
Chemical composition of the AA6082 alloy [41].

Composition	Si	Fe	Cu	Mn	Mg	Cr	Zn	Ti	Al
Percentage (wt. -%)	0.7 ~ 1.3%	0.5%	0.1%	0.4 ~ 1.0%	0.6 ~ 1.2%	0.25%	0.20%	0.10%	Balanced

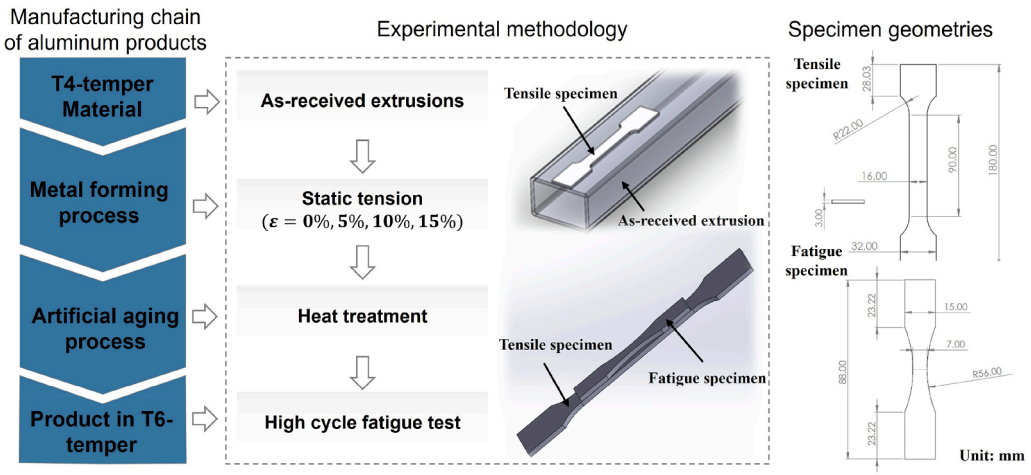

Fig. 2. Schematic illustration of the experimental methodology for simulating the manufacturing process; the geometrical dimensions of the static and fatigue specimens (right).

deformation and subsequent artificial ageing examined by uniaxial tensile tests are shown in Fig. 3. Here, 'base material' refers to the as-received AA6082 in stable T4-temper. The results show that the initial yield strength increases with the pre-strain introduced prior to ageing. The opposite tendency is observed for the fracture strain, which clearly decreases with increased pre-ageing deformation.

The tensile properties of the AA6082 samples in T6-temper with different pre-strain levels are shown in Fig. 4. The ultimate stress, initial yield stress, uniform elongation (prior to distributed necking), and fracture elongation are shown with engineering values. With a higher pre-strain, this implies that higher initial yield and ultimate stresses are obtained. The total elongation after fracture decreases with increased pre-strain, showing reduced 'ductility' with respect to the increased pre-strain.

Compared to the specimens without pre-strain, the yield strength increases 4.6%, 6.8% and 7.9% with a pre-strain of 5%, 10% and 15% applied before ageing, respectively. From these static tensile test results, a value of 250 MPa (about 90% of the yield strength of the sample without pre-strain) is chosen as the proper stress range for all the fatigue tests. Due to the slight increase of the yield strength with respect to the pre-strain, the stress range corresponds to approximately 83–85% of the yield strength of the pre-strained samples.

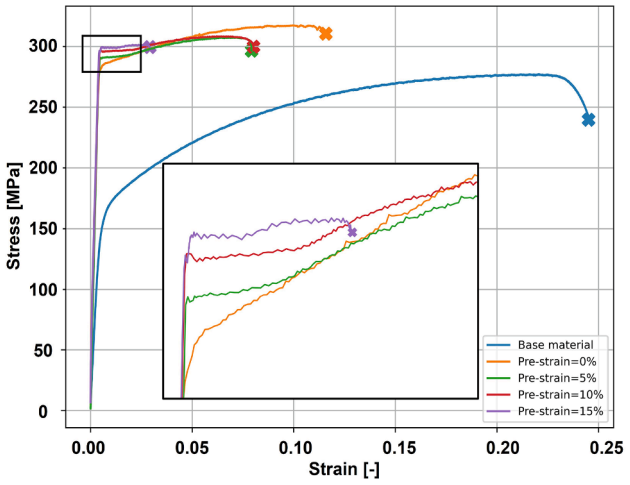

Fig. 3. Engineering stress-strain curves for specimens with different pre-strain levels. The fracture point is marked with a cross.

3.2. High-cycle fatigue behavior

3.2.1. Fatigue life cycles

Load-controlled HCF tests are conducted for the pre-deformed and aged specimens. The pre-strained specimens are heat-treated in one single batch to ensure the same thermal exposure. The fracture location in the tests is shown for a selected assortment of specimens in Fig. 5. Abnormal fracture locations do occasionally appear in the fatigue tests, as indicated by the black arrow in Fig. 5 e). Note that the data obtained from abnormal specimens are not included in the results.

A boxplot of the fatigue life cycles is shown in Fig. 6. It should be noted that the test results of specimens with the maximum and minimum fatigue life are not included for providing more reliable results. Despite the relatively few samples, the 'statistical' minimum, first quartile, median, third quartile, and maximum fatigue life cycles are marked in the plot. The raw data is displayed with the dots. The relative difference of median fatigue life cycles between each pre-strain level and undeformed samples are also plotted with orange squares and shown as a full line.

As shown in Fig. 6, the median fatigue life of pre-strained samples is extended as compared to the undeformed samples. The increments of fatigue cycles are 18.6%, 22.1% and 23.9% with pre-strain levels of 5%, 10% and 15%, respectively, as compared to the undeformed specimen. When the pre-strain is increased from 5% to 15%, the fatigue life tends to slightly increase, yet with limited magnitude, say, only 5%.

Employing SEM of the fracture surface, the crack origin area, propagation area and fracture area could be clearly distinguished, as shown in Fig. 7. The mechanism of the fatigue process can be explained accordingly. In the tested AA6082-T6 samples, the grain shapes, precipitations, and void formation have suffered from the simulated thermal-mechanical history. Once the fatigue tests start, the slip systems are activated from the formed dislocations during the loading stage. The dislocations slip under the shear strains from the uniaxial tension. In the crack origin area, the dislocation motions are obstructed by grain boundaries, precipitates, or voids, therefore causing potential nucleation of the fatigue crack. With the cyclic loading, the accumulation of irreversible dislocation slips initiates a micro-crack at the nucleation site. In this sample, fracture features along the grain boundaries are formed (marked by arrows in the figure). Depending on the pre-strain level, the nucleation of the crack could locate on the grain boundaries or within the grain. Then, the further cyclic loading promotes crack propagation with micro-plasticity accumulation at the crack tip. At each cycle, the micro-crack develops a certain distance, indicated by the striations normal to the loading direction. Finally, ductile fracture takes place due to the deteriorated specimen strength, represented as the

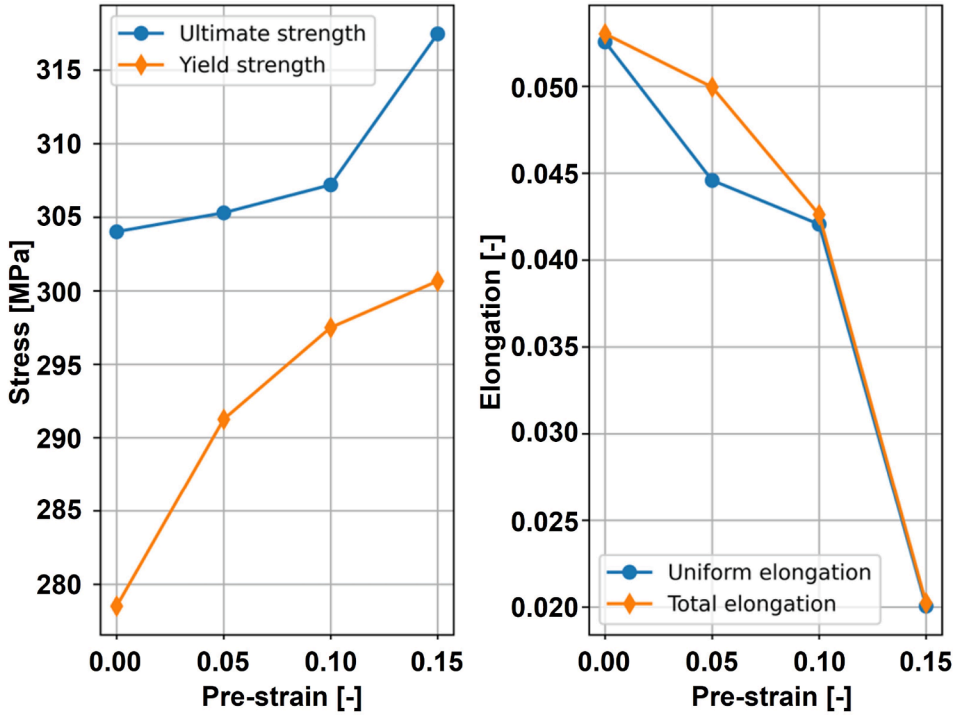

Fig. 4. The static properties of AA6082-T6 with different pre-strain levels are shown on the left and the corresponding elongation on the right.

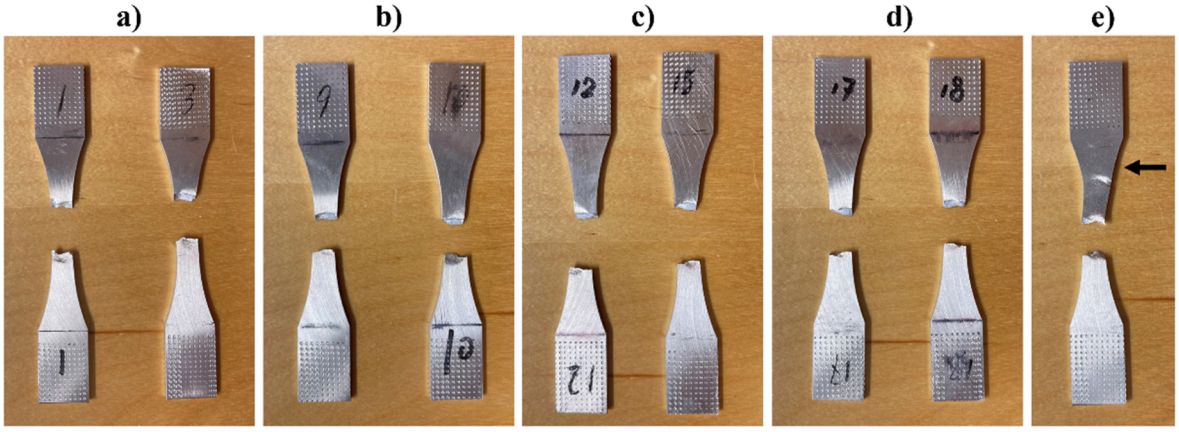

Fig. 5. Photographs revealing the fracture location of selected specimens in HCF tests; a) 0% pre-strain (no pre-strain), b) 5% pre-strain, c) 10% pre-strain, d) 15% pre-strain, e) abnormal fracture location.

typical dimple structures. The plastic deformation increases substantially in this stage and the dimples correspond to voids nucleated from inclusions. The microstructures are the same as that of the fracture surface from the static tensile test. The comparison reveals that the fracture mechanics are different in the two tests. When the local plasticity is accumulated gradually and cyclically in the HCF tests, there will be less nucleation and more significant crack development. On the contrary, the substantial plastic deformation in the static tensile tests results in more nucleation and less crack development.

For specimens with no or a relatively low pre-strain level (0% and 5%), intergranular fracture features can be observed, as shown in Fig. 8 (a) and (b), and Fig. 9 (a) and (b). This phenomenon is due to the stage I crack growth associated with the single slip systems [44]. In this stage, the dislocation slip is the dominant mechanism, and the single slip system is mainly activated in the crystallites in the aluminium alloy. The directions of dislocation slipping planes become more specific and limited by the crystallographic orientations. The Burgers vector has to be a translation vector of the crystal which – except for very special cases – does not hold for the neighbor crystal due to the difference in orientation [45]. When the dislocations travel to a grain boundary, it becomes difficult to get across the boundary to another grain. As a result, these dislocations will accumulate at the boundaries, which accordingly cause strain incompatibility between different grains after a certain number of cycles. Therefore, the localized concertation of dislocations would result in microscale damage (or micro-cracks) formed along the grain boundaries in the material under cyclic loading. Then, the initiated crack develops further into the stage II crack growth, which is conducted by multiple slip systems [44]. When the slips are impeded by un-shearable precipitates, the plasticity accumulates along the line of intersection of slip systems, thus forming the fatigue striations on the fracture surface.

For the samples with a higher pre-strain level (10% and 15%), as shown in Fig. 8 (c) and (d), and Fig. 9 (c) and (d), the intergranular fracture features are less visible, if present at all. In these cases, the multiple slip systems have activated in the early stage of cyclic loading

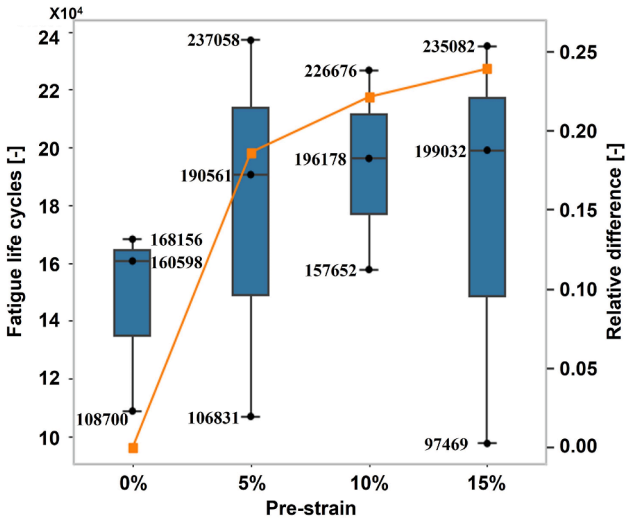

Fig. 6. Box plot of the fatigue life test results and relative difference (full orange line) of statistical median fatigue life cycles compared to undeformed samples.

for the pre-strained material. The crack initiates as stage II crack growth directly and the stage I crack growth may be absent, consequently showing mainly even fatigue striations in the crack origin area. The crystallites have already been re-orientated to accommodate the increased macroscopic strain. Moreover, the incompatibility along the grain boundaries has been reduced. The constraints from the specific slip systems (local crystallography) become less significant. Thus, the generated micro-cracks will not develop along the incompatible grain boundaries, showing fewer intergranular fracture features on the fractured surface of the fatigue specimens. In addition, a higher pre-strain level impacts the nucleation rate and number density of the precipitation during the ageing process [46]. It increases the possibility of crack initiation within the grains.

The change of fracture mechanism is believed to be an important root cause of the increased fatigue life for the specimens with a larger pre-strain level. It has been found in literature that more dissipated energy is needed for the transgranular fracture mode than the intergranular fracture, and that the fracture toughness increases with a larger fraction of transgranular fracture [47]. Thus, the fatigue life can increase with more transgranular fracture, as this replaces the intergranular fracture when larger pre-strains are introduced. The variation of the fatigue life with the same pre-strain level is also possibly linked to the fracture features. The time of the crack initiation and development is influenced by the portion of dominated fracture features. This is consistent with the observed trend of higher fatigue life with fewer intergranular fracture features from the fracture surfaces, especially for pre-strain levels of 0% and 5%. It should be noted that the strain hardening effect may also play an important role in increasing the fatigue life cycles. It is harder to accumulate local plasticity for the pre-strained material during fatigue, and this effect becomes more noticeable with an increasing pre-strain.

The variation of the fatigue life is found to increase with the larger pre-strain level in this work. The same phenomenon was observed by Staley et al. [16] for A206-T71 aluminum castings with hot isostatic pressing (HIP). In their study, the elongation induced by HIP was found to increase the average and maximum fatigue life of the material, yet at the expense of a large variation of fatigue life. It was also explained that more cracks initiating from the surface contribute to the decrease of fatigue life. According to the work by Reis et al. [29], the variation of fatigue life could be related to the different crack initiation positions. It is found that the fracture surfaces of specimens of 2198 Al-Li alloy showed mainly precipitates and micro-voids while failing after a few cycles, whereas the specimens with a higher number of fatigue cycles showed cracks that initiated at the surface. In this work, the link between fatigue life cycles and crack initiation mentioned above is less obvious. Thus, the change of fracture mechanism and the strain hardening effects from the introduced pre-strain may contribute to the improved fatigue life. As for the cases with significantly reduced fatigue life, this may be related to micro-voids in the material. The possibility of micro-void formation and the fraction of micro-voids might be increased under large plastic deformation. Micro-plasticity during cyclic loading tends to accumulate more easily with these micro-voids present, meaning that the crack development rate increases, and the fatigue life decreases. The SEM results of the specimen pre-strained at 15% (with a higher and lower fatigue life) are shown in Fig. 10, focusing on the

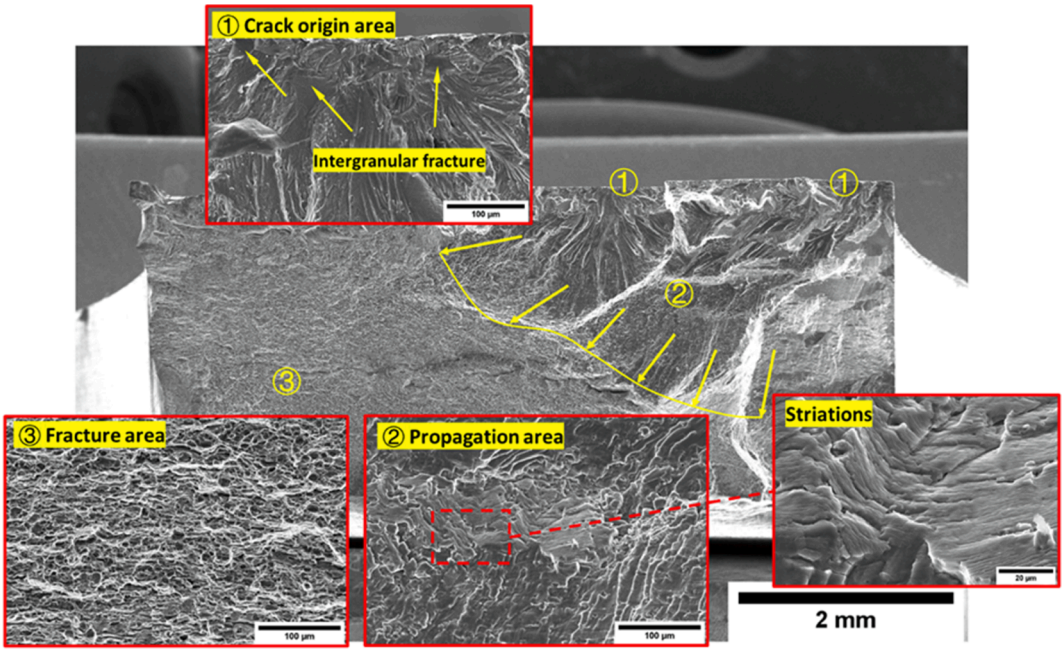

Fig. 7. Illustration of fracture in the fatigue test samples.

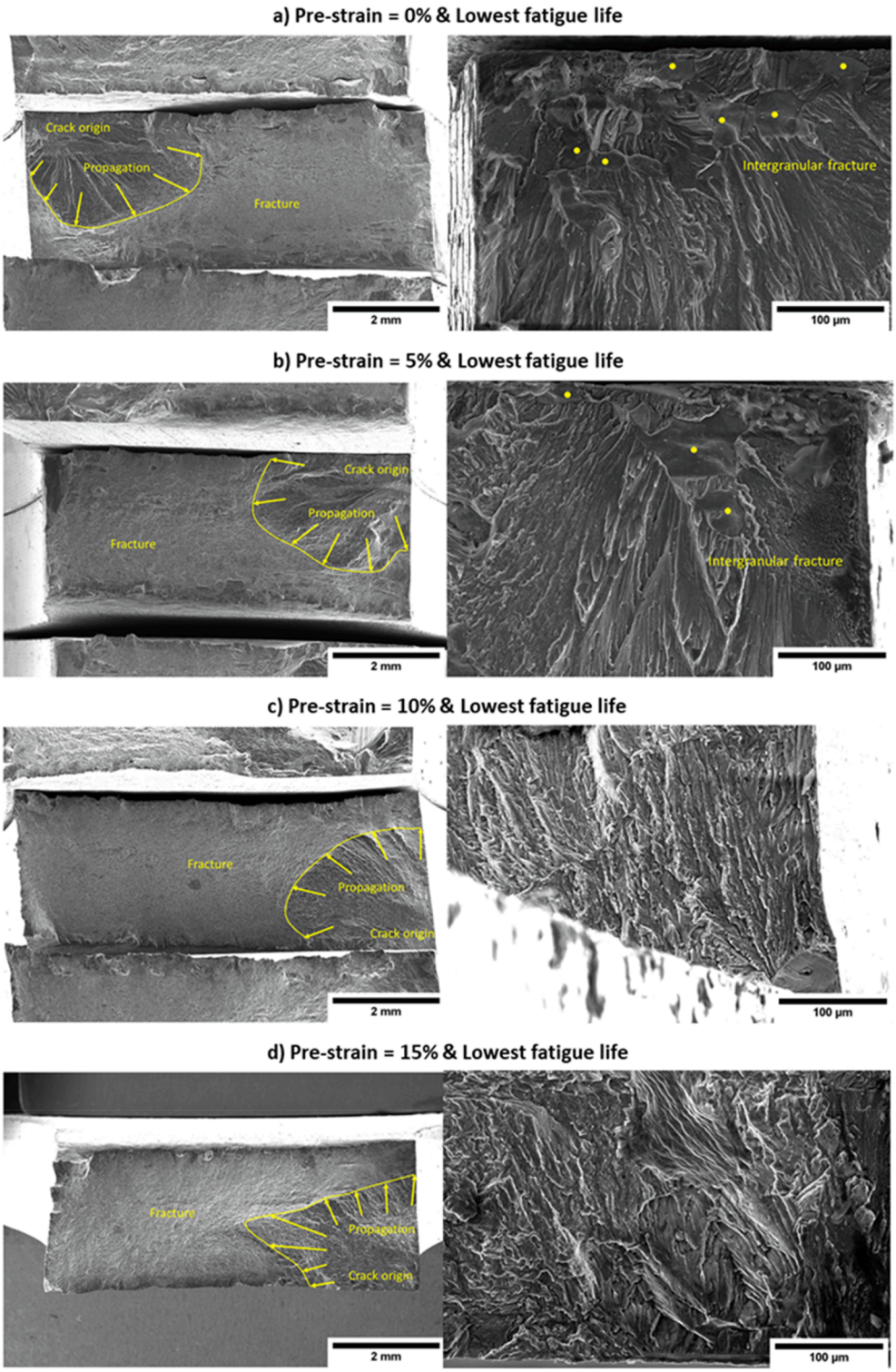

Fig. 8. Fracture surfaces of fatigue specimens (lowest fatigue life) observed by SEM.

propagation area. The fracture surface of the specimen with the shorter fatigue life (top) shows more local strain concentrations than the specimen with a longer fatigue life (bottom).

The test results obtained herein are also compared to the fatigue design codes of aluminum profiles. The S-N curves from the Eurocode [48] for plane members are used. Curves are defined by two parameters, $\Delta\sigma_c$ and m_1, meaning the fatigue strength and constant amplitude fatigue limit at 2×10^6 cycles, respectively. For AA6082 extrusions, category 71–7 ($\Delta\sigma_c$-m_1) is suggested, according to the standard. An enhancement factor of 1.16 should be used to scale the $\Delta\sigma_c$ due to the set stress ratio. Thus, category 85.2–7 (blue lines) is shown with standard categories (red lines) in Fig. 11.

Compared to the scaled category (85.2–7), the fatigue life cycles of the samples are mostly larger than the value given by the curve in Eurocode. A few cases may give non-conservative results compared to the scaled category. However, the standard category in red should be used in the real design stage. Considering the variation of the material properties and manufacturing process, a standard design curve 80–7,

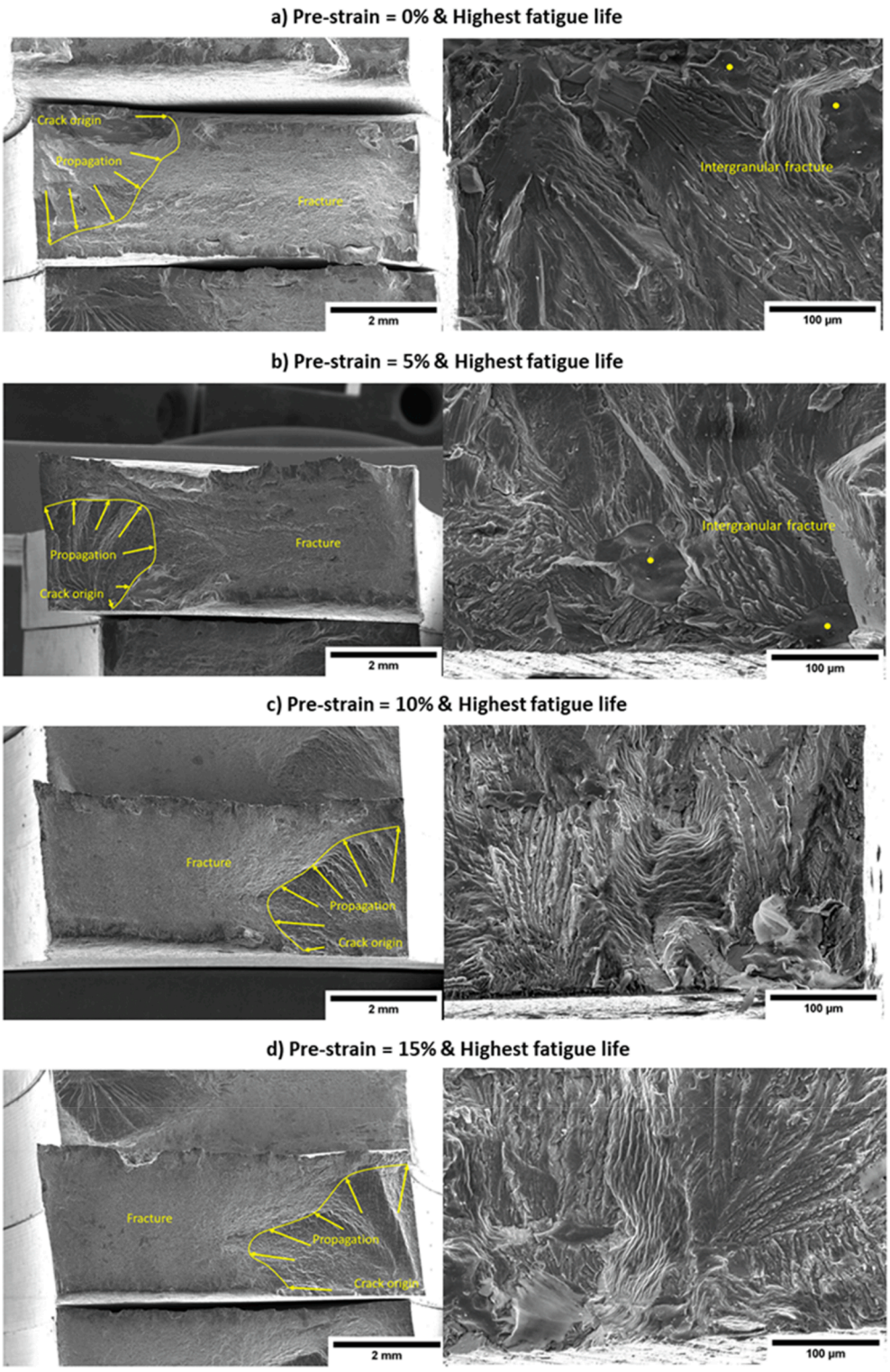

Fig. 9. Fracture surfaces of fatigue specimens (highest fatigue life) observed by SEM.

with slightly lower $\Delta\sigma_c$ than the scale category, can provide a conservative fatigue design. It is suggested that the category given by the Eurocode could be conservatively applied to the extruded AA6082-T6 material with the simulated thermo-mechanical processing route employed in this work.

3.2.2. Cyclic stress-strain behavior

In the HCF tests, as mentioned above, the stress range is constant. In each stress cycle, the strain value ε and the corresponding mean strain ε_{mean} could be calculated as follows:

$$\varepsilon = \frac{D}{L_0} \tag{1}$$

$$\varepsilon_{mean} = \frac{\varepsilon_{\max} + \varepsilon_{\min}}{2} \tag{2}$$

where

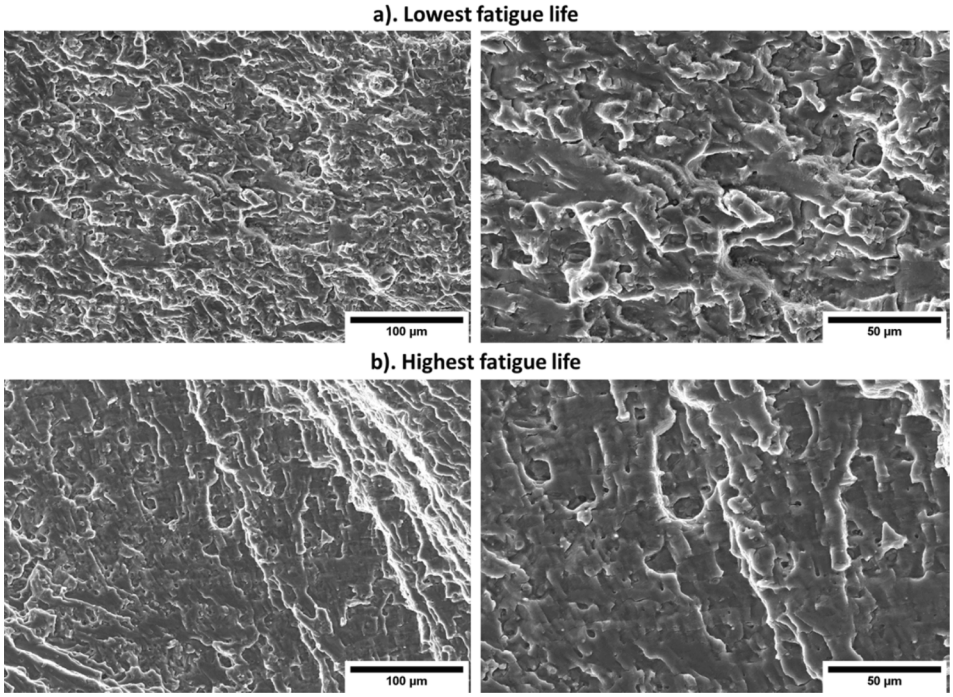

Fig. 10. SEM focusing on the propagation area of the specimens pre-strained at 15% with the higher and lower fatigue life.

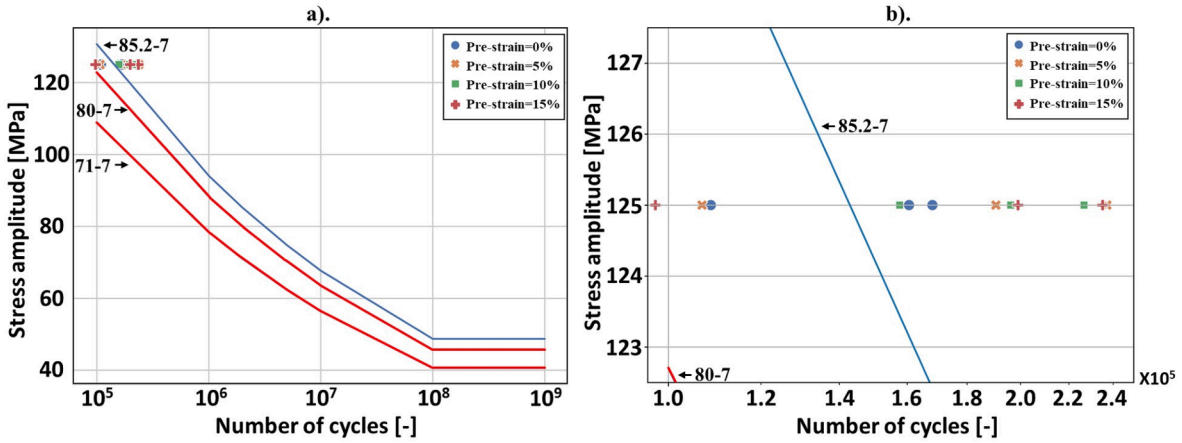

Fig. 11. Fatigue life comparison between test results and current design curves. A zoomed view is given in b). The test results with different pre-strain levels are scattered with different markers and colors.

D is the measured axial displacement,

L_0 is the distance between two radius segments of the fatigue specimen,

ε_{max} is the maximum strain of each cycle,

and ε_{min} is the minimum strain of each cycle.

The mean strain of each fatigue cycle is plotted with the normalized fatigue life in Fig. 12. The fatigue life is normalized according to the ratio of the counted cycle and total fatigue life cycle. Hence, the normalized fatigue life '0′ and '1′ mean the first and last cycle of the fatigue tests, respectively. Compared to the value at the beginning of the fatigue tests, the increased mean strain denotes cyclic softening behavior, while the decreased value means cyclic hardening behavior, due to the consistent stress amplitude in the fatigue tests.

For all tested specimens, softening behavior is observed at the early beginning of the fatigue test and followed by a cyclic hardening phenomenon in most of the cases. The material yields the highest strength with cyclic hardening. After this, the material softens until a fracture occurs. It is worth noting that the specimens present different cyclic deformation behaviors even with the same pre-strain level. The observed difference in the crack initiation and development of the tested specimens in Fig. 8 leads to this phenomenon, which is in accordance with the observations made by Reis et al. [29] for AA2024 aluminum alloys.

To compare the cyclic material behavior, the degree of cyclic softening is introduced and defined as follows:

$$D_{softening} = \frac{\varepsilon_{mean_i} - \varepsilon_{mean_0}}{\varepsilon_{mean_0}} \tag{3}$$

where

ε_{meani} is the mean strain at the i-th cycle,

ε_{meano} is the mean strain at the first cycle.

Thus, a positive $D_{softening}$ value indicates a softer material compared to the one in the initial state, while a negative $D_{softening}$ value means a harder one.

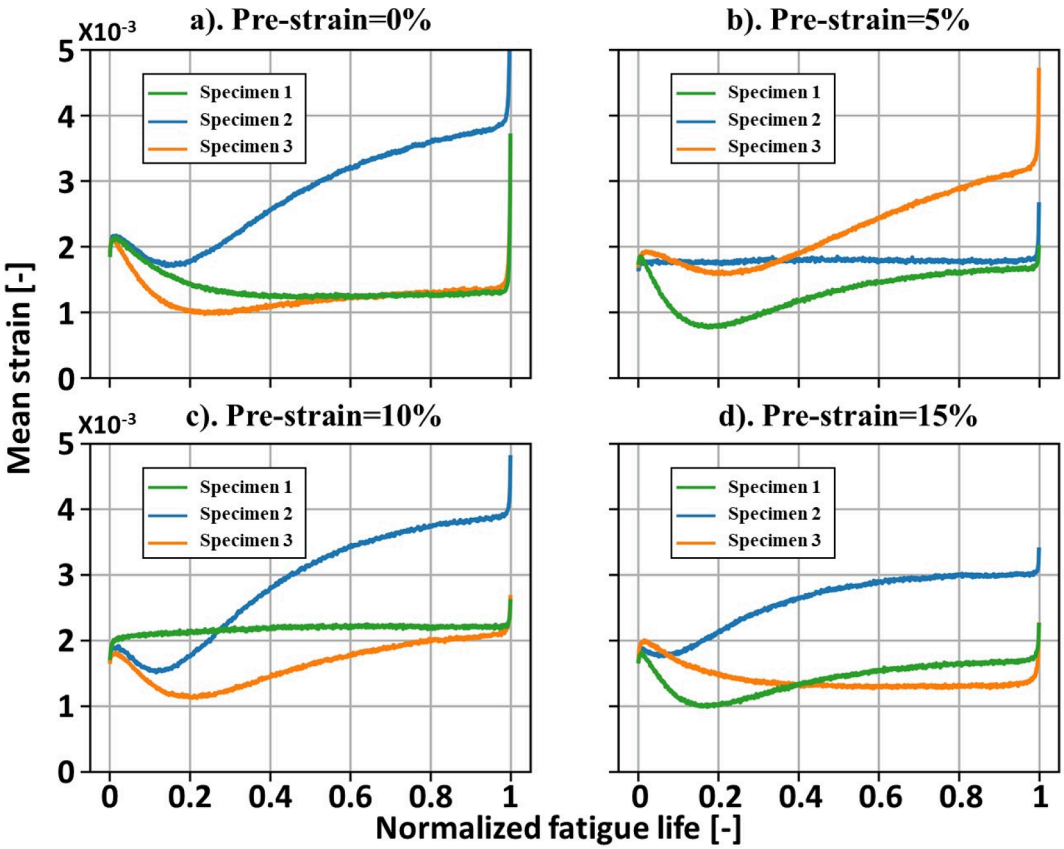

Fig. 12. Plot of the mean strain during fatigue life; a) Pre-strain 0% (no pre-strain), b) pre-strain 5%, c) pre-strain 10%, d) pre-strain 15%. Different specimens are shown in different colors.

Fig. 13 illustrates the degree of cyclic softening for different fatigue tests. The normalized fatigue life is displayed with a logarithmic axis to provide a focus on the very beginning stage. The specimens with the same pre-strain level are grouped in (a)-(d). For all the specimens, the softening behavior is significant in the beginning. The material gets softer than its initial state, independent of the pre-strain level. However, this trend shifts and is only observed for 0.01 to 0.05 of the total fatigue life. Then, a significant hardening stage can be identified for the vast majority of the specimens. The duration of hardening may vary between specimens, but normally occupies a large portion of the fatigue life. The material becomes harder than in its initial state with cyclic hardening. The degree of cyclic hardening might be up to 50% as shown in Fig. 13. Beyond the cyclic hardening range, the material once again experiences cyclic softening until the final fracture. In some cases, indicated with arrows in b) and c), the material shows only dynamic softening, yielding a softer material than the initial state during the whole fatigue life.

The degree of cyclic softening for specimens with different pre-strain levels is averaged and compared in Fig. 14. The beginning and main portion of the fatigue life are focused on as shown in Fig. 14 a) and b), respectively. The reduction of the hardening magnitude with the pre-strain is obvious, as indicated by the solid arrows. The pre-strained material is softer than the non-deformed material in most of the fatigue lifetime. From the pre-strain level of 0% to 10%, a trend of increased softening can be observed. It is noticed that the material with pre-strain level of 15% becomes harder than that with pre-strain level of 10%, rather than showing further softening, as indicated by the dashed arrows. As for the initial softening stage, the duration and magnitude are basically similar for the specimens with different pre-strain levels, as shown in the zoomed view of a). A larger softening magnitude for the material with 5% pre-strain and a longer softening interval for the material with 10% pre-strain can be observed. However, the deviation could possibly stem from natural variations in material microstructures. The existence of an initial softening stage regardless of the pre-strain level still could be concluded.

For the AA6082-T6 aluminum alloys under pre-strain and subsequent artificial ageing, the fatigue life can be divided into three stages based on the characteristic of fatigue cyclic behavior. A summarized curve of the degree of cyclic softening is shown in Fig. 15. In the initial stage, the material demonstrates cyclic softening, extending around 1% of the fatigue life. Then, a cyclic hardening stage appears and dominates 10–20% of the fatigue life. The cyclic softening degree is decreased from a positive 'peak' to a negative 'valley' in this stage, revealing material from a softer state to a harder state compared to that at the beginning of the first stage. In the third stage, the material softens again until the final fracture. The degree of material softening increases from the negative 'valley' toward zero or even a positive value, depending on the deformation history. An introduction of the pre-strain tends to increase the magnitude of cyclic softening during the fatigue tests. The second stage with the cyclic hardening is shortened and the degree of the softening is increased, as indicated by the arrows in Fig. 15.

The cyclic hardening behavior of the material is assumed highly related to the nature and stability of dislocation substructures [49,50]. Aluminum alloy AA6082-T6 is generally associated with cyclic softening behavior [51], while peak aged A319 alloys show a more complex cyclic behavior including initial hardening, steady stage and then cyclic softening at lower total strain amplitude, [30]. It has also been reported that cyclic hardening is followed by softening till the end for the 6082 alloys after cryorolling and room temperature rolling, whether the material is being annealed or not [28]. The studied material in the present research shows a mixed cyclic behavior under coupled effects of pre-strain and subsequent post-thermal-treatment. In addition to the hardening-softening behavior mentioned above, transient softening is observed at

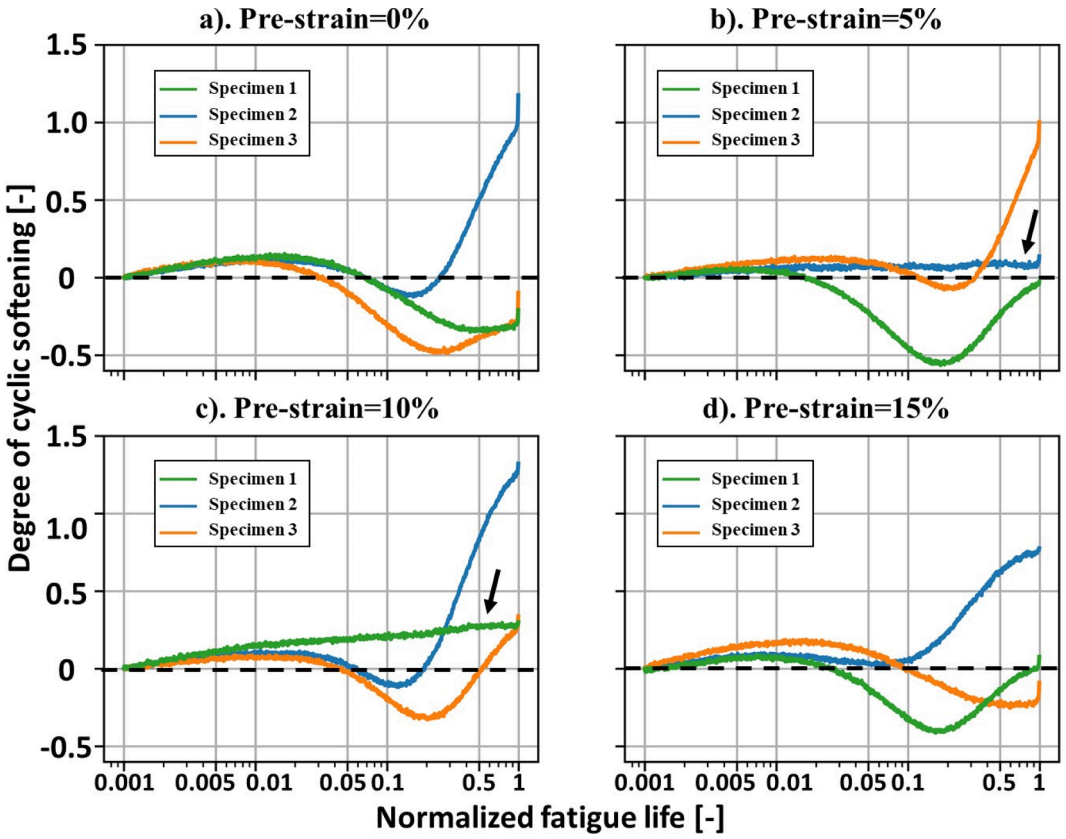

Fig. 13. Plots of cyclic softening behavior during fatigue life using a logarithmic x-axis.

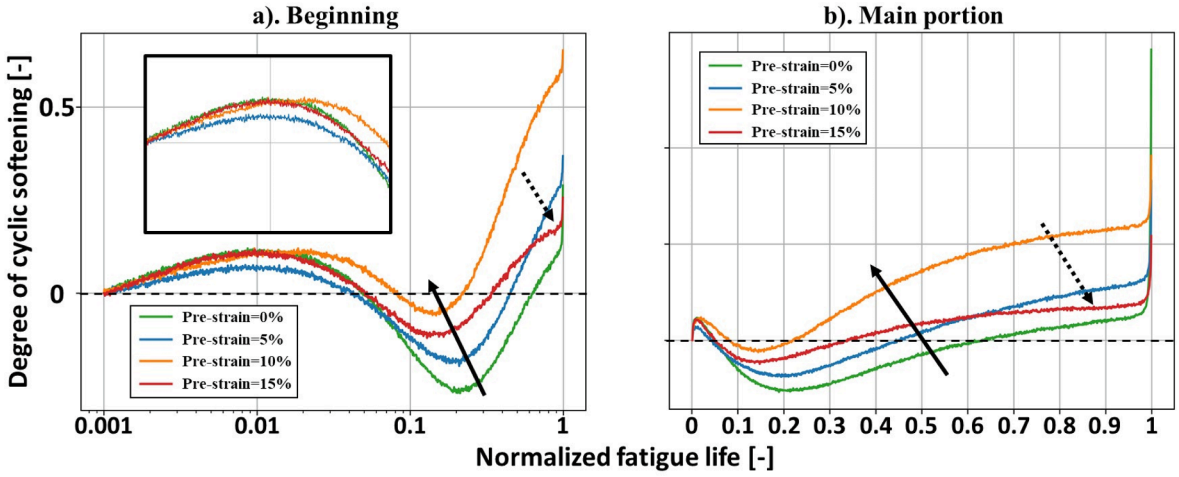

Fig. 14. Plots of the averaged degree of cyclic softening for each pre-strain level.

the very early stage of fatigue life. This may be related to the increased dislocation density after pre-deformation and post-thermal treatment. The subsequent strain cycling rearranges the dislocations to provide less resistance to deformation, resulting in cyclic softening of the material. Then, with the accumulation of cyclic plastic strain, the dislocation density increases again, which results in significant cyclic hardening. Finally, the crack occurrence and development soften the material until fracture finally occurs.

Based on the SEM fractography, the softening behavior and the microstructural change can be linked. A schematic illustration is shown in Fig. 15: In the initial stage, the dislocation slip systems, which are activated by the designed manufacturing process, are rearranged in the crystallites to give less resistance. As a result, cyclic softening occurs. In the second stage, local plasticity is accumulated to trigger intergranular or transgranular fracture. The material demonstrates cyclic hardening with such accumulation. In the final stage, a crack has been initiated and further development results in cyclic softening behavior. The striations in the propagation area may represent this stage. The entire process resembles fatigue failure stages in the case of ductile face-centered (FCC) metals; namely, strain localization, crack initiation, crack propagation and fatigue failure [52]. However, advanced experiments such as in-situ SEM are necessary to investigate the link in detail.

The introduced pre-strain may result in a significant increase in cyclic softening during fatigue. Such a phenomenon is also closely related

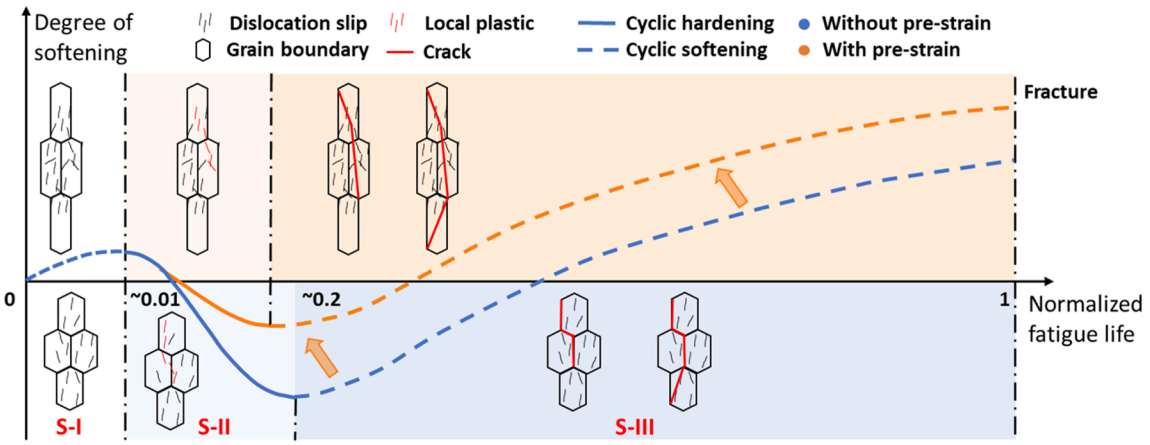

Fig. 15. Illustration of the cyclic behavior of AA6082 aluminum alloy with the designed manufacturing process and pulsating loading conditions. Three stages are indicted by 'S-I', 'S-II' and 'S-III'.

to the large dislocation density, which promotes the development of cracking [50], yielding softening of the material during cyclic loading. The mechanism of cyclic softening of AA6082 alloys was also investigated by Kumar et al. [28,53]. In their works, the large secondary phase particles and decreasing fraction of low angle grain boundaries were assumed being the main reason for softening. The same mechanism may also prevail for the tested material in this study because the pre-strain can accelerate particle precipitations [46] and change the grain boundary angles.

The thermo-mechanical history simulated in this study includes pre-strain in T4-temper and post-thermal treatment to T6-temper. All specimens are subjected to tensile pulsating loading scenarios. The history effects on the fatigue behavior of AA6082 alloys and related mechanisms can be summarized as follows: The pre-strain accelerates the nucleation rate and increases the number density of precipitations during artificial aging. The resulting multiple slip systems change the dominated fracture mechanism from intergranular fracture to transgranular fracture. The crack initiation is also changed to stage II crack growth mainly, skipping the stage I crack growth. A larger portion of transgranular fracture induced by the pre-strain causes larger fracture toughness, thus increasing the fatigue life, together with the reduced local micro-plasticity accumulation from strain hardening. However, the introduced pre-strain may also increase the occurrence of micro-void due to more precipitations, thus leading to a local strain concentration and substantially reduced fatigue life in some cases. The level of cyclic softening behavior is somehow proportional to pre-strain levels within the range from 0% to 10%. A value of 15% tends to harden the material instead of providing further softening. It is believed that the large dislocation density due to the pre-strain can promote crack development and subsequent material softening. Artificial ageing is the main reason for the initial softening phenomenon considering that the cyclic softening behavior in this stage is insensitive to pre-strain levels. Overall, the fatigue life is increased by pre-straining but at a cost of larger variation. This study has demonstrated that the material behaves in three cyclic stages, i.e., softening-hardening-softening.

4. Conclusions and outlooks

The fatigue behavior of AA6082-T6 aluminum alloy with pre-deformation induced in T4-temper was investigated using HCF tests and SEM analysis. The main conclusions from this study are summarized as follows:

(1). The fatigue life is extended 18–23% by pre-strain in T4-temper for AA6082-T6 alloy, resulting in a larger median fatigue life cycle. The pre-deformed aluminum components could provide equal or better fatigue performance than unformed components prior to ageing.
(2). The dominated mechanism of fatigue fracture is changed from intergranular fracture to transgranular fracture when increasing the level of pre-straining in T4-temper. The activated multiple slip systems may reduce the stress–strain concentration from incompatible grain boundaries, hence increasing the fatigue life.
(3). The investigated AA6082 aluminum alloy shows a three-stage cyclic phenomenon under pulsating loading conditions. These stages include a transient softening stage, a cyclic hardening stage, and a cyclic softening stage until the final fracture. Different stages can be linked to microstructural development during cyclic loading.
(4). The introduced pre-strain results in more significant cyclic softening during the entire fatigue lifetime of the material. An increasing trend of softening is found by increased pre-strain from 0% to 10%; however, a pre-strain level of 15% will harden the material.

This study mainly investigated the fatigue behavior of AA6082 alloys that have undergone several simulated processing routes. We acknowledge that the obtained conclusions are tentative since the thermo-mechanic effects in industrial manufacturing processes are interrelated and complex. In additon, the actual working conditions of components are more complex than the description in this work. Therefore, more fatigue experiments coving a wider range of stress amplitudes and stress ratios are suggested to provide a more generic and in-depth understanding of how the processing history affects fatigue behavior of AA8082-T6 profiles. Finally, in order to link the cyclic softening behavior and the microstructural change in detail, it is recommended to use in-site SEM in future work.

Declaration of Competing Interest

The authors declare that they have no known competing financial interests or personal relationships that could have appeared to influence the work reported in this paper.

Acknowledgements

The authors gratefully acknowledge the support from AdaptAl (Adaptive Control of Aluminum Manufacturing) with project number 314054, funded by Hydro ASA and The Research Council of Norway. Thanks also go to NTNU Aluminum Product Innovation Center (NAPIC) and NTNU Centre for Autonomous Marine Operations and Systems (AMOS). In addition, the authors would like to thank Prof. F. Berto, Prof.

J. Amdahl, and Dr. S.M.J. Razavi at NTNU for their insightful suggestions in this work, and special thanks to Dr. D. Wan at NTNU for his help with the SEM test and analysis.

References

[1] Kheradmand AB, Tayebi M, Akbari MM, Abbasian A. Effect of quench-controlled precipitation hardening on microstructure and mechanical properties of Al-Zn-Mg-Cu-Zr alloys contain of Sc micro-alloying. J Alloy Compd 2022/05/05/ 2022;902:163748. https://doi.org/10.1016/j.jallcom.2022.163748.

[2] Scharifi E, Savaci U, Kavaklioglu ZB, Weidig U, Turan S, Steinhoff K. Effect of thermo-mechanical processing on quench-induced precipitates morphology and mechanical properties in high strength AA7075 aluminum alloy. Mater Charact 2021/04/01/ 2021;174:111026. https://doi.org/10.1016/j.matchar.2021.111026.

[3] Ma W-Y, Wang B-Y, Lin J-G, Tang X-F. Influence of process parameters on properties of AA6082 in hot forming process. Trans Nonferr Metals Soc China 2017/11/01/ 2017;27(11):2454–63. https://doi.org/10.1016/S1003-6326(17)60272-3.

[4] Scharifi E, Knoth R, Weidig U. Thermo-mechanical forming procedure of high strength Aluminum sheet with improved mechanical properties and process efficiency. Procedia Manuf 2019/01/01/ 2019;29:481–9. https://doi.org/10.1016/j.promfg.2019.02.165.

[5] Wang W, Pan Q, Wang X, Sun Y, Long L, Huang Z. Mechanical properties and microstructure evolution of ultra-high strength Al-Zn-Mg-Cu alloy processed by room temperature ECAP with post aging. Mater Sci Eng: A 2018/07/25/ 2018;731:195–208. https://doi.org/10.1016/j.msea.2018.06.047.

[6] Cepeda-Jiménez CM, García-Infanta JM, Ruano OA, Carreño F. Mechanical properties at room temperature of an Al–Zn–Mg–Cu alloy processed by equal channel angular pressing. J Alloy Compd 2011/09/01/ 2011;509(35):8649–56. https://doi.org/10.1016/j.jallcom.2011.06.070.

[7] Liu J, Li S, Li D, Yang R. Effect of aging on fatigue-crack growth behavior of a high-temperature titanium alloy. Mater Trans 2004;45(5):1577–85. https://doi.org/10.2320/matertrans.45.1577.

[8] Zhu SC, Lu XF, Gong JM. Effect of pre-deformation and ageing on compressive behavior of Ti-58.25wt%Ni alloys at room temperature. Adv Mater Res 2011;197–198:375–82. https://doi.org/10.4028/www.scientific.net/AMR.197-198.375.

[9] Osaki K, Kikuchi S, Nakai Y, Kawabata MO, Ameyama K. The effects of thermo-mechanical processing on fatigue crack propagation in commercially pure titanium with a harmonic structure. Mater Sci Eng: A 2020/01/31/ 2020;773:138892. https://doi.org/10.1016/j.msea.2019.138892.

[10] Hockauf K, Wagner MFX, Halle T, Niendorf T, Hockauf M, Lampke T. Influence of precipitates on low-cycle fatigue and crack growth behavior in an ultrafine-grained aluminum alloy. Acta Mater 2014/11/01/ 2014;80:250–63. https://doi.org/10.1016/j.actamat.2014.07.061.

[11] Ghalehbandi SM, Fallahi-Arezodar A, Hosseini-Toudeshky H. Fatigue crack growth resistance of 7075 Al alloy after equal channel angular pressing. Fatigue Fract Eng Mater Struct 2016;39(12):1517–25. https://doi.org/10.1111/ffe.12472.

[12] Sajadifar SV, Scharifi E, Wegener T, Krochmal M, Lotz S, Steinhoff K, et al. On the low-cycle fatigue behavior of thermo-mechanically processed high-strength aluminum alloys. Int J Fatigue 2022;156:106676. https://doi.org/10.1016/j.ijfatigue.2021.106676.

[13] Hattori CS, Almeida GFC, Gonçalves RLP, Santos RG, Souza RC, da Silva WC, et al. Microstructure and fatigue properties of extruded aluminum alloys 7046 and 7108 for automotive applications. J Mater Res Technol 2021;14:2970–81. https://doi.org/10.1016/j.jmrt.2021.08.085.

[14] Nourian-Avval A, Fatemi A. "Fatigue design with high pressure die cast aluminum including the effects of defects, section size, stress gradient, and mean stress". Mater Today Commun 2020/12/01/ 2020;25:101567. https://doi.org/10.1016/j.mtcomm.2020.101567.

[15] Nourian-Avval A, Fatemi A. Fatigue life prediction of cast aluminum alloy based on porosity characteristics. Theor Appl Fract Mech 2020/10/01/ 2020;109:102774. https://doi.org/10.1016/j.tafmec.2020.102774.

[16] Staley JT, Tiryakioğlu M, Campbell J. The effect of hot isostatic pressing (HIP) on the fatigue life of A206–T71 aluminum castings. Mater Sci Eng: A 2007/09/15/ 2007;465(1):136–45. https://doi.org/10.1016/j.msea.2007.02.009.

[17] Tiryakioğlu M. On the relationship between elongation and fatigue life in A206–T71 aluminum castings. Mater Sci Eng: A 2014/04/17/ 2014;601:116–22. https://doi.org/10.1016/j.msea.2014.02.033.

[18] Branco R, Borrego LP, Costa JD, Antunes FV. Effect of pre-strain on cyclic plastic behaviour of 7050–T6 aluminium alloy. Procedia Struct Integrity 2019;17:177–82. https://doi.org/10.1016/j.prostr.2019.08.024.

[19] Branco R, Costa JD, Borrego LP, Wu SC, Long XY, Antunes FV. Effect of tensile pre-strain on low-cycle fatigue behaviour of 7050–T6 aluminium alloy. Eng Fail Anal 2020/08/01/ 2020;114:104592. https://doi.org/10.1016/j.engfailanal.2020.104592.

[20] Al-Rubaie KS, Del Grande MA, Travessa DN, Cardoso KR. Effect of pre-strain on the fatigue life of 7050–T7451 aluminium alloy. Mater Sci Eng: A 2007/08/25/ 2007;464(1):141–50. https://doi.org/10.1016/j.msea.2007.02.024.

[21] Froustey C, Lataillade JL. Influence of large pre-straining of aluminium alloys on their residual fatigue resistance. Int J Fatigue 2008/05/01/ 2008;30(5):908–16. https://doi.org/10.1016/j.ijfatigue.2007.06.011.

[22] Arora PR, Raghavan MR. Effect of tensile prestrain on fatigue strength of aluminum alloy in high cycle fatigue. J Eng Mater Technol 1973;95(2):76–82. https://doi.org/10.1115/1.3443135.

[23] Kariya M, Hatano K, Horibe S. Influence of compressive pre-strain on tensile fatigue in two types of aluminum alloys. J Mater Eng Perform 2010/11/01 2010;19(8):1205–7. https://doi.org/10.1007/s11665-010-9594-4.

[24] Chen Y, Zhou J, Liu C, Wang F. Effect of pre-deformation on the pre-corrosion multiaxial fatigue behaviors of 2024–T4 aluminum alloy. Int J Fatigue 2018/03/01/ 2018;108:35–46. https://doi.org/10.1016/j.ijfatigue.2017.11.008.

[25] Chen YQ, Zhang H, Pan SP, Song YF, Liu X, Liu WH. "Effects of service environment and pre-deformation on the fatigue behaviour of 2524 aluminium alloy". Arch Civil Mech Eng 2019/12/18 2019;20(1):5. https://doi.org/10.1007/s43452-019-0002-z.

[26] Bekheet NE, Gadelrab RM, Salah MF, Abd El-Azim AN. "The effects of aging on the hardness and fatigue behavior of 2024 Al alloy/SiC composites". Mater Des 2002/04/01/ 2002;23(2):153–9. https://doi.org/10.1016/S0261-3069(01)00072-3.

[27] Leng L, Zhang ZJ, Duan QQ, Zhang P, Zhang ZF. Improving the fatigue strength of 7075 alloy through aging. Mater Sci Eng: A 2018/12/19/ 2018;738:24–30. https://doi.org/10.1016/j.msea.2018.09.047.

[28] Kumar N, Goel S, Jayaganthan R, Owolabi GM. The influence of metallurgical factors on low cycle fatigue behavior of ultra-fine grained 6082 Al alloy. Int J Fatigue 2018/05/01/ 2018;110:130–43. https://doi.org/10.1016/j.ijfatigue.2018.01.018.

[29] Reis DAP, Couto AA, Domingues Jr NI, Hirschmann AC, Zepka S, de Moura Neto C. "Effect of Artificial aging on the mechanical properties of an aerospace aluminum alloy 2024". Defect Diffusion Forum 2012;326–328:193–8. https://doi.org/10.4028/www.scientific.net/DDF.326-328.193.

[30] Tian DD, Liu XS, He GQ, Shen Y, Lv SQ, Wang QG. Low cycle fatigue behavior of casting A319 alloy under two different aging conditions. Mater Sci Eng: A 2016/01/27/ 2016;654:60–8. https://doi.org/10.1016/j.msea.2015.12.023.

[31] Haskel T, Verran GO, Barbieri R. Rotating and bending fatigue behavior of A356 aluminum alloy: effects of strontium addition and T6 heat treatment. Int J Fatigue 2018/09/01/ 2018;114:1–10. https://doi.org/10.1016/j.ijfatigue.2018.04.012.

[32] Rezanezhad S, Azadi M, Azadi M. Influence of heat treatment on high-cycle fatigue and fracture behaviors of piston aluminum alloy under fully-reversed cyclic bending. Met Mater Int 2019;27(5):1–11.

[33] Z. Shan *et al.*, "Mechanism of Precipitate Microstructure Affecting Fatigue Behavior of 7020 Aluminum Alloy," *Materials,* vol. 13, no. 15, p. 3248, 2020. [Online]. Available: https://www.mdpi.com/1996-1944/13/15/3248.

[34] Khisheh S, Khalili K, Azadi M, Hendouabadi VZ. Influences of roughness and heat treatment on high-cycle bending fatigue properties of A380 aluminum alloy under stress-controlled cyclic loading. Mater Chem Phys 2021/05/01/ 2021;264:124475. https://doi.org/10.1016/j.matchemphys.2021.124475.

[35] Hockauf K, Niendorf T, Wagner S, Halle T, Meyer LW. Cyclic behavior and microstructural stability of ultrafine-grained AA6060 under strain-controlled fatigue. Procedia Eng 2010/04/01/ 2010;2(1):2199–208. https://doi.org/10.1016/j.proeng.2010.03.236.

[36] Larichkin A, Zakharchenko K, Gorev B, Kapustin V, Maksimovskiy E. Influence of the creep ageing process on the fatigue properties of components from V95pchT2 (analog 7175T76) and V95ochT2 (analog 7475) aluminium alloys. J Phys Conf Ser 2017/10 2017;894:012050. https://doi.org/10.1088/1742-6596/894/1/012050.

[37] Liu F, Liu Z, Liu M, Hu Y, Chen Y, Bai S. Analysis of empirical relation between microstructure, texture evolution and fatigue properties of an Al-Cu-Li alloy during different pre-deformation processes. Mater Sci Eng: A 2018/05/30/ 2018;726:309–19. https://doi.org/10.1016/j.msea.2018.04.047.

[38] Zhang Y, Ling J, Li H-G, Luo X-Y, Ba Z-X. Effect of pre-deformation and artificial aging on fatigue life of 2198 Al-Li alloy. Mater Res Express 2020;7(4):046509. https://doi.org/10.1088/2053-1591/ab83a6.

[39] Zheng K, Politis DJ, Wang L, Lin J. A review on forming techniques for manufacturing lightweight complex—shaped aluminium panel components. Int J Lightweight Mater Manuf 2018/06/01/ 2018;1(2):55–80. https://doi.org/10.1016/j.ijlmm.2018.03.006.

[40] Welo T, Ringen G, Ma J. An overview and evaluation of alternative forming processes for complex aluminium products. Procedia Manuf 2020/01/01/ 2020;48:82–9. https://doi.org/10.1016/j.promfg.2020.05.022.

[41] Hydro. "Technical datasheet - Extruded products Alloy EN AW-6082 [AlSi1MgMn]." Hydro Innovation & Technology. (accessed).

[42] Ma J, Welo T, Wan D. The impact of thermo-mechanical processing routes on product quality in integrated aluminium tube bending process. J Manuf Processes 2021/07/01/ 2021;67:503–12. https://doi.org/10.1016/j.jmapro.2021.05.015.

[43] A. Designation, "E466-07, Standard practice for conducting force controlled constant amplitude axial fatigue tests of metallic materials," *ASTM International,* 2007.

[44] Künkler B, Düber O, Köster P, Krupp U, Fritzen CP, Christ HJ. Modelling of short crack propagation – transition from stage I to stage II. Eng Fract Mech 2008/02/01/ 2008;75(3):715–25. https://doi.org/10.1016/j.engfracmech.2007.02.018.

[45] Gottstein G. Physical foundations of materials science. Springer Science & Business Media; 2013.

[46] Li JF, Chen YL, Zhang XH, Zheng ZQ. Role of pre-deformation on aging precipitation behavior of Al-Cu-Li alloys. Mater Sci Forum 2017;877:180–7. https://doi.org/10.4028/www.scientific.net/MSF.877.180.

[47] Kawabata T, Izumi O. the relationship between fracture toughness and transgranular fracture in an Al-6.0% Zn-2.5% Mg alloy. Acta Metall 1977/05/01/ 1977;25(5):505–12. https://doi.org/10.1016/0001-6160(77)90190-0.

[48] C. Eurocode, "9: Design of aluminium structures-Part 1-3: Structures susceptible to fatigue," 1999: Eurocode.

[49] Hertzberg RW. Deformation and fracture mechanics of engineering materials. 3rd ed. New York: Wiley; 1989.
[50] Bannantine JA, Comer JJ, Handrock JL. Fundamentals of metal fatigue analysis. Englewood Cliffs, N.J: Prentice Hall; 1990.
[51] Borrego LP, Abreu LM, Costa JM, Ferreira JM. Analysis of low cycle fatigue in AlMgSi aluminium alloys. Eng Fail Anal 2004/10/01/ 2004;11(5):715–25. https://doi.org/10.1016/j.engfailanal.2003.09.003.
[52] H. Mughrabi, "Microstructural mechanisms of cyclic deformation, fatigue crack initiation and early crack growth," *Philosophical Transactions of the Royal Society A: Mathematical, Physical and Engineering Sciences,* vol. 373, no. 2038, p. 20140132, 2015.
[53] Kumar N, Goel S, Jayaganthan R, Brokmeier H-G. Effect of grain boundary misorientaton, deformation temperature and AlFeMnSi-phase on fatigue life of 6082 Al alloy. Mater Charact 2017/02/01/ 2017;124:229–40. https://doi.org/10.1016/j.matchar.2017.01.002.